ICAS 2020 SHANGHAI
International Council of the Aeronautical Sciences
32nd Congress of the International Council of the Aeronautical Sciences
September 6-10, 2021
Pudong Shangri-La, Shanghai, China

DRAG REDUCTION ANALYSIS IN CLOSE-FORMATION FLIGHT

Xiaoxuan Meng[1], Min Chang[2], Junqiang Bai[2], Ming Li[1]

[1]School of Aeronautics, Northwestern Polytechnical University, Xi'an, China, 710072
[2]Unmanned System Research Institute, Northwestern Polytechnical University, Xi'an, China, 710072

Abstract

Formation flight, especially the close-formation flight, can reduce the drag and increase the flight range by using the wake vortices in a beneficial way. Therefore, it is important to study the phenomenon of drag reduction of vortex flow in close-formation flight. In this paper, two flying-wings were chosen to form the close-formation, and the cruise aerodynamics of the close-formation were analyzed by changing the relative position of two aircrafts, and the reasons for these variations of aerodynamic characteristics were further analyzed. The study found that the lead aircraft in close-formation is almost unaffected by the tail aircraft, and the cruise drag reduction of tail aircraft mainly comes from its reduction of the cruise angle of attack because of the upwash flow of the wake vortices. The cruise drag is minimal when the lead aircraft and the tail aircraft overlap about 10% wing span; The violent increase or decrease of aerodynamic load deviation relative to the single air-craft due to wake vortices, especially in wing head aero, causes the violent decrease or increase of the pitching moment of the aircraft.

Keywords: close formation; vortex flow; drag reduction; aerodynamic load.

1. Introduction

The concept of 'vortex surfing' was put forward in order to reduce the drag of the follower using the wake vortex from captain in multi-aircraft formation flight and improve the economy of the formation. However, the risk of the formation flight is increased due to the existence of the wake vortex. The generation, development to final dissipation of the wake vortex will make the flow field more complicated, which is harmful to flight control. Many scholars noticed the formation flight and had made a lot of effort on its potential benefits and practical application in the past years.

The study of formation flight can be traced back to a century ago. The phenomenon of the formation flying among the birds had been noticed widely at that time, such as the V-shaped flying formation composed of the wild goose and the cloud-flight formed by starling clusters[1]. Wiseelsberger is the first aerodynamic scholar to study the formation flying of the birds from the view point of aerodynamics using the lifting-line theory, which proved that the formation flying can improve the overall aerodynamic performance of the formation. Lissaman [2] has studied the formation flying of the 25 birds in 1970, the average energy saving for the formation can be up to 71% compared to a bird. In 1983, Hummel [3] pointed out that the longitudinal interval among birds has little effect on the overall aerodynamic performance, while the spread interval has a great effect on the aerodynamic performance in bird formation.

Inspired by bird formation flying, some scholars began to study the formation flight of the aircraft. The flight tests of the formation flight were carried out and the advantages of the drag reduction for formation were proved. In 1996, the in-flight measurements were performed on two Dornier 28 aircraft in formation flight, and about 15% fuel saving for the follower was measured[4]. Wagner et al. [5] reported the flight-test results of two Northrop T-38 Talon aircraft in formation, and revealed that it is possible to achieve an average 8% fuel saving for the follower. The flight tests with two F/A-18 aircraft in formation were conducted by NASA and the test demonstrated a maximum fuel saving of 18% for the follower [6]. The U.S. Air Force Research Laboratory has been investigating the potential benefits

for formation of C-17 aircrafts in the Surfing Aircraft Vortices for Energy (SAVE) project. The average fuel saving for the follower can be up to 7–9% in the project [7,8].

In addition to flight tests of formation, the numerical simulations can provide more insight in the formation flight. In 1977, Maskew [9] studied the formation effect of the wings with large aspect ratio on the aerodynamics of each wing using the Vortex Lattice Method (VLM). The results also show that the formation of 3 to 5 aircrafts can increase the flight range of the overall formation by up to 46% to 67%. In 2000, Blake [10] analyzed the aerodynamic characteristics of follower in close formation using horseshoe vortex model with viscous vortex core that can effectively reflect the aerodynamic coupling effect caused by wake vortex interaction between aircrafts. Ning et al. [11] showed that a reduction of approximately 30% in induced drag can be achieved in a two-aircraft formation. Veldhuis et al. [12] used a vortex lattice method to estimate the reduction in induced drag in trimmed flight. The typical values calculated for the reduction in induced drag for the trailing aircraft in a two-aircraft formation were 60%. Slotnick [13] analyzed the different formation and obtained more detail information, such as the contour of the formation drag distribution in space, using the VLM and the modern CFD numerical method. The development and evolution of wake vortex along the flow direction are numerically simulated. Zhang et al. [14] developed a new computationally efficient aerodynamic model for close formation using lifting-line theory with the accuracy close to the fundamental VLM, the effects of the many factors on the drag reductions are investigated. Based on Prandtl lifting lines theory and a simplified equation of motion, Caprace et al. [15] in 2019 developed the wake vortex detection and tracking model using Ensemble Kalman Filter for aircraft formation flight, which can be used to provide the follower with the optimal location for maximizing the benefits of the formation flight.

Multiple UAV formation has gradually become the main air combat style of major military powers, the new distributed combat system of system of UAVs can adapt better to complex and fierce battle environment. Although there are still great difficulties in realizing the close formation flight at the present, the huge advantages of aerodynamic and combat for formation flight have been promoting many researchers to carry out the in-depth study on it. In this paper, two flying wing UAV were chose to form the close formation, the drag reduction analysis and the sensitivity analysis of the aerodynamic performance of the aircrafts in formation about the formation parameters was carried out using VLM numerical method. The reasons for these variations of aerodynamic characteristics were further analyzed with the introduction of the aerodynamic load distribution on the wing.

2. Numerical Approach

The Vortex Lattice Method (VLM) is one of the earliest methods used to estimate the aerodynamics of the aircraft, and it is an effective numerical method for solving the lifting surface theory. It is based on the solution of Laplace equation with the outstanding advantages of clear physical concept. The VLM is used to carry out the aerodynamics sensitivity analysis of the formation parameters in close formation flight due to its efficient calculation and acceptable accuracy. The Reynolds Average Navier-Stokes (RANS) equation solver is chose to provide the results of aerodynamics with high precision in order to compare with the result of VLM and check its accuracy.

2.1 Vortex Lattice Method

In order to obtained the aerodynamics of the lift surface through VLM, the plane of the lift surface is divided into many grids with the horseshoe vortexes attached it, and the vortex lines of the horseshoe vortexes are arranged along the quarter-chord direction at each grid with two semi-infinite long vortex filaments running parallel to x axis at the end of the lines, which is called the vortex lattices. The strength of the horseshoe vortexes attached these grids are determined by satisfying the wall boundary conditions at the control points located at the three-quarter-chord on each grid.

2.1.1 *The linear equations of the circulation distribution on the wing*

The induced velocity at the point P in space for a horseshoe vortex with strength Γ is expressed as

a three-component dimensionless form along the *x*, *y*, *z* direction through the introduction of the dimensionless circulation $\gamma = \Gamma / bV$, as follow:

$$\begin{cases} \dfrac{u}{V}(x,y,z) = Ku(x_1,y_1,z_1;x_2,y_2,z_2;x,y,z)\cdot\gamma \\ \dfrac{v}{V}(x,y,z) = Kv(x_1,y_1,z_1;x_2,y_2,z_2;x,y,z)\cdot\gamma \\ \dfrac{w}{V}(x,y,z) = Kw(x_1,y_1,z_1;x_2,y_2,z_2;x,y,z)\cdot\gamma \end{cases} \tag{1}$$

where *b* is the span of the wing, the *u*, *v*, *w* is the component of the velocity along the *x*, *y*, *z* direction respectively, *V* is the value of the velocity of free flow at infinity, *Ku*, *Kv*, *Kw* is called the three component of the coefficient of the influence and its the physical meaning is the dimensionless induced velocity at the point (*x*, *y*, *z*) for the horseshoe vortex with the dimensionless circulation strength of 1. It is only a function of coordinates of the grid on the wing, which can be obtained after the coordinates of horseshoe vortexes and control points are determined.

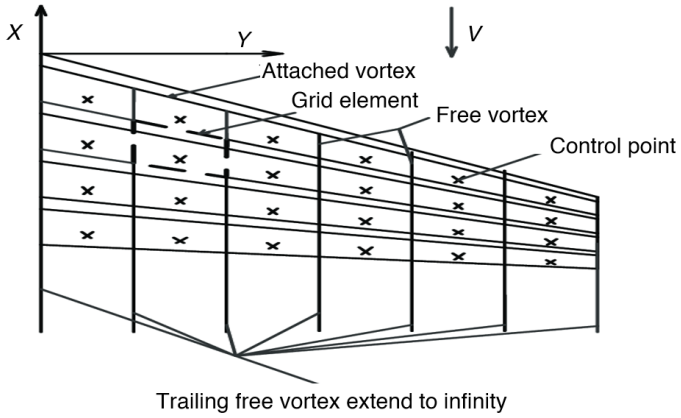

Figure 1 – Schematic of the Vortex Lattice Method

The wing is divided into a grid with the size of RR×SS with meaning that there is RR×SS horseshoe vortexes on the wing. The total induced velocity of all horseshoe vortices at the control point of the *i*-th grid can be described as

$$\begin{cases} \dfrac{u_i}{V}(x,y,z) = \sum\limits_{j=1}^{RR\times SS} Ku_{ij}\gamma_j \\ \dfrac{v_i}{V}(x,y,z) = \sum\limits_{j=1}^{RR\times SS} Kv_{ij}\gamma_j \\ \dfrac{w_i}{V}(x,y,z) = \sum\limits_{j=1}^{RR\times SS} Kw_{ij}\gamma_j \end{cases} \tag{2}$$

where the *i* is represented the *i*-th control point to calculated induced velocity, and the *j* is represented the *j*-th grid with the horseshoe vortex attached. The u_{ij}, v_{ij}, w_{ij} are the induced velocity components at the *i*-th control point induced by the horseshoe vortex on the corresponding *j*-th grid.

When the dihedral angle ψ is not 0, the normal induced velocity can be expressed as follow:

$$\frac{v_{ni}}{V} = \sum_{j=1}^{RR\times SS} \left(Kw_{ij}\cos\psi - Kv_{ij}\sin\psi\right)\gamma_j = \sum_{j=1}^{RR\times SS} D_{ij}\gamma_j \tag{3}$$

According to the boundary conditions that the air flow at the control point must be tangent to the mid-arc surface of the wing, then:

$$\sum_{j=1}^{RR\times SS} D_{ij}\gamma_j = -\left\{\alpha - \left(dz/dx\right)_i + \delta\right\} = \alpha_i, \left(i = 1,2,L,RR\times SS\right) \tag{4}$$

where α is the local AoA, $(dz/dx)_i$ the slope of the middle arc line and δ is the deflection angle of the control surface (which is required to be positive when the control surface deflects downward).

Then, the RR×SS-dimensional linear equations system about the unknown quantity, the circulation on the wing γ, can be obtained and written in matrix form as

$$[D]\{\gamma\} = \{\alpha\} \tag{5}$$

By solving the solution, the circulation distribution of the wing is obtained as follow:

$$\{\gamma\} = [D]^{-1}\{\alpha\} \tag{6}$$

2.1.2 *The Aerodynamic coefficients of the wing*

The aerodynamic coefficients that is relevant to the lift can be easily solved after the circulation distribution on the wing is obtained. For the lift that acted on the grid elements of the wing, it is equal the force on the attached vortex line and can be expressed as:

$$L_j = \left|\rho \boldsymbol{V}\times\Gamma_j \boldsymbol{l}_j\right| = \rho V\Gamma_j l_j sin\left(\boldsymbol{V},\boldsymbol{l}_j\right) = \rho V\Gamma_j l_j cos\Lambda_j = \rho V^2 b\bar{\Gamma}_j \Delta y_j \tag{7}$$

where L_j is the lift on the j-th grid element, the ρ is the density of the air in the flow field, the $\boldsymbol{V}$ is the velocity of free flow at infinity, Λ_j and l_j are the sweep angle and the length of the attached vortex line, the b is the span of the wing, Δy_j is the span of the j-th grid element, the Γ_j is the circulation on the j-th grid element, and the corresponding dimensionless circulation on the j-th grid element is defined as:

$$\bar{\Gamma}_j = \Gamma_j / Vb \tag{8}$$

The coefficient of the lift at the y profile $C_L(y)$ along the spread direction can be expressed as:

$$C_L(y) = \sum_{j=1}^{SS} \frac{\rho V^2 b\bar{\Gamma}_j \Delta y_j}{0.5\rho V^2 c(y)\Delta y_j} = \frac{2b}{c(y)}\sum_{j=1}^{SS}\bar{\Gamma}_j \tag{9}$$

where the $c(y)$ is the local chord at the y profile on the wing, SS is the quantity of the rows of the grid on the half wing. Then, the coefficient of the lift on the wing can be obtained as follow:

$$C_L = 2\sum_{j=1}^{RR} \frac{C_L(y)_j\, 0.5\rho V^2 c(y)_j\, \Delta y_j}{0.5\rho V^2 S_w} = \frac{2}{S_w}\sum_{j=1}^{RR} C_L(y)_j\, c(y)_j\, \Delta y_j \tag{10}$$

where the S_w is the aera of the wing, RR is the quantity of the columns of the grid on the half wing.

The coefficient of the drag at the y profile $C_D(y)$ along the spread direction can be expressed as:

$$C_D(y) = \sum_{j=1}^{SS} \frac{\rho Vb\bar{\Gamma}_j w_j \Delta y_j}{0.5\rho V^2 c(y)\Delta y_j} = \frac{2b}{Vc(y)}\sum_{j=1}^{SS}\bar{\Gamma}_j w_j \tag{11}$$

Then, the coefficient of the drag C_D on the wing can be obtained as follow:

$$C_D = 2\sum_{j=1}^{RR} \frac{C_D(y)_j\, 0.5\rho V^2 c(y)_j\, \Delta y_j}{0.5\rho V^2 S_w} = \frac{2}{S_w}\sum_{j=1}^{RR} C_D(y)_j\, c(y)_j\, \Delta y_j \tag{12}$$

The coefficient of the pitch moment around the y axis at the y profile $C_M(y)$ along the spread direction can be expressed as:

$$C_M(y) = \sum_{j=1}^{SS} \frac{\rho V^2 b\bar{\Gamma}_j \Delta y_j x_{bj}}{0.5\rho V^2 c^2(y)\Delta y_j} = -\frac{2b}{c^2(y)}\sum_{j=1}^{SS}\bar{\Gamma}_j x_{bj} \tag{13}$$

where the x_{bj} is the x coordinates of the mid-point of the attached vortex line. Then, the coefficient of the pitch moment C_M on the wing can be obtained as follow:

$$C_M = 2\sum_{j=1}^{RR} \frac{C_M(y)_j\, 0.5\rho V^2 c^2(y)_j\, \Delta y_j}{0.5\rho V^2 S_w c_A} = \frac{2}{S_w c_A}\sum_{j=1}^{RR} C_M(y)_j\, c^2(y)_j\, \Delta y_j \tag{14}$$

where the C_A is the mean aerodynamic chord (MAC) of the wing.

After the lift that acted on each grid element of the wing is obtained, we can obtain the aerodynamic load distribution acted on the mid-arc surface of the wing that is reflected the magnitude of lift in each position of the wing. With the aera S_j and the lift L_j of the j-th grid element, the aerodynamic load on this grid element can be converted to the dimensionless quantity, the coefficient of aerodynamic load $(C_{PL})_j$, it can be written as:

$$(C_{PL})_j = \frac{L_j}{0.5\rho V^2 S_j} = \frac{\rho V^2 b\bar{\Gamma}_j \Delta y_j}{0.5\rho V^2 \Delta x_j \Delta y_j} = \frac{2b\bar{\Gamma}_j}{\Delta x_j} \tag{15}$$

where the S_j is the area of the j-th grid element and Δx_j is the mean chord of the j-th grid element, the $(C_{PL})_j$ is acted on the midpoint of the attached vortex line on the grid element generally. The aerodynamic load C_{PL} solved by VLM is equivalent to the Cp difference between the upper and lower surface of the wing at the same position solved by RANS at the same position, which can be written as:

$$C_{PL} = \Delta Cp = (Cp)_{low} - (Cp)_{up} \tag{16}$$

where the *low* and *up* represent the lower and upper surface of the wing.

2.2 The validation of VLM

M6 is a wing model designed by ONERA, and a series of wind tunnel tests on the model are carried out under transonic conditions. It was tested in a wind tunnel at transonic Mach numbers (0.7, 0.84, 0.88, 0.92) and various angles-of-attack (AoA) up to 6°. The Reynolds numbers were about 12 million based on the MAC. The ONERA-M6 wing model is selected to verify the accuracy of VLM in subsonic flow. The geometry of the ONERA-M6 and its structural mesh with the quantity up to 1.8 million to calculation are shown in Figure 2.

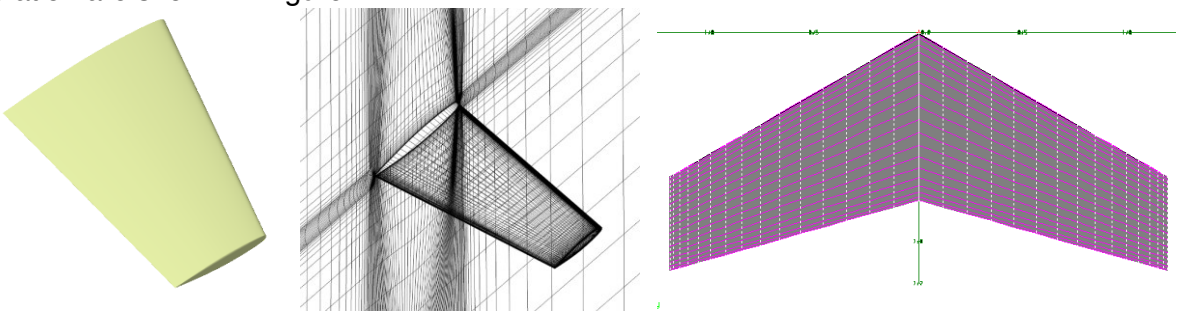

(a) geometry (b) mesh for RANS (c) mesh for VLM

Figure 2 – The geometry and mesh of ONERA-M6

The condition at the subsonic flow is set for the ONERA-M6 wing as follows: the Mach number Ma=0.5, the Reynolds number Re=6.98×10^6 based on MAC, the AoA with the range from -3° to 2°. Its aerodynamic characteristics is obtained using VLM and RANS, as shown in Figure 3, and the circulation distributions at same lift on them are shown in Figure 4. It can be found that the results of VLM are nearly consistent to those of RANS before the wing gets stalled though the lift solved by VLM is slightly less than RANS. Compared to the circulation distributions on the wing along the spread direction obtained using VLM and RANS, it can be seen that the circulation distribution obtained by VLM is in good agreement with that of RANS in the inner wing except that there is a small difference in the outer wing. Therefore, it can be verified that, the accuracy of VLM can be guaranteed with the certain credibility in the range of small AoA at the subsonic flow.

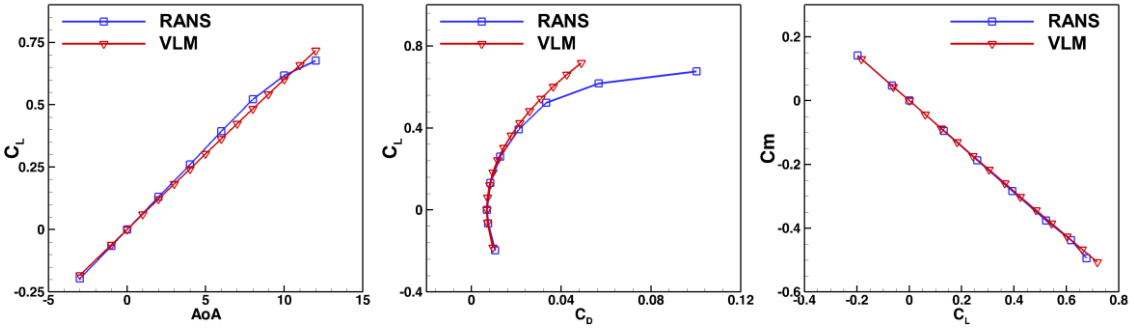

(a) AoA-C_L (b) C_L-C_D (c) C_L-C_m

Figure 3 – The aerodynamic characteristics of ONERA-M6 wing using VLM and RANS

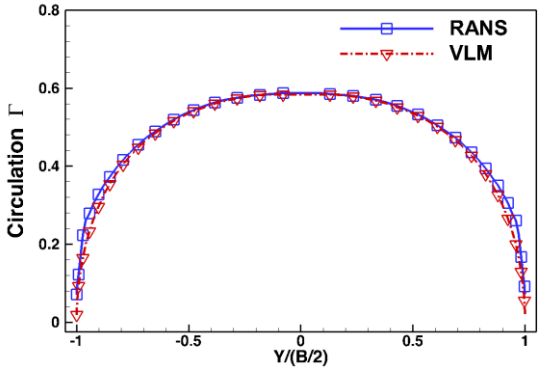

Figure 4 – The circulation distribution of ONERA-M6 wing at same lift using VLM and RANS

The aerodynamic load distributions at the same AoA condition solved by VLM and RANS at some profiles on the ONERA-M6 wing are given in Figure 5 in order to verify the accuracy of the VLM. As we can see, the maximum aerodynamic load is appeared on the head of the wing, and the aerodynamic load is decreased gradually along the chord direction. On the head of the wing where the shape of the wing has the great influence on the aerodynamic performance, the aerodynamic load solved by VLM is less than the results of RANS because the geometry model used in VLM cannot reflect the real physics shape of the wing, which caused a little lift loss by VLM at the same AoA condition. Further, the phenomenon that the aerodynamic load is decreased on the head of the wing but is increased slightly on the tail of the wing makes the pitch moment on the wing solved by VLM decreased. Compared with the aerodynamic load solved by VLM and RANS, the results of VLM are close to those of RANS, which meanings that VLM can capture to the magnitude distribution of aerodynamic load on the wing.

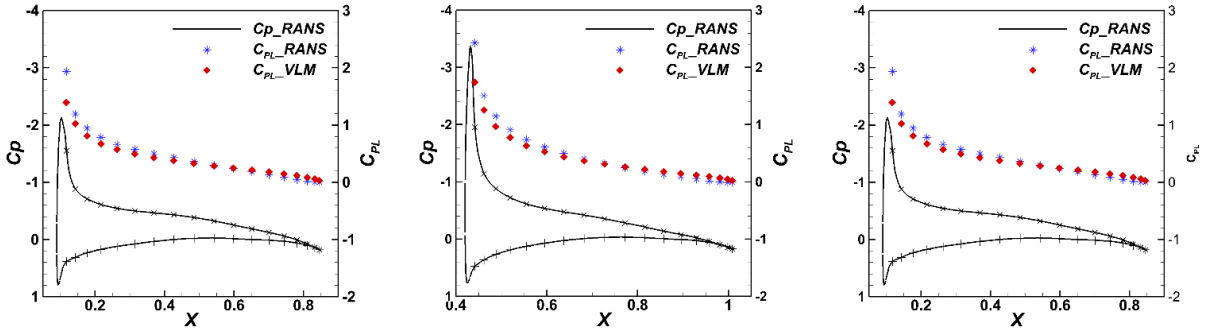

(a) Y=0.15m (b) Y=0.72m (c) Y=1.10m

Figure 5 – The pressure and aerodynamic load distribution of the ONERA-M6 wing

2.3 Aerodynamics of the Flying Wing

The blended wing body configuration, called flying-wing, has a clear aerodynamic shape with high aerodynamic efficiency. The flying-wing has no additional components such as horizontal and vertical

tail, and the additional aerodynamic influence caused by these components will not be introduced in formation flight, therefore the flying-wing configuration is chose to study its aerodynamic in multi-aircraft close formation flight.

The geometry and mesh of the flying-wing are shown in the Figure 6, the span of flying wing is 10.829m, the length is 6.579m, the refer area is 30.2 m^2, and the length of MAC is 3.793m. The aerodynamic for the single flying wing is obtained using VLM, and verified through RANS. The flow conditions are as follows: the free flow Mach number Ma=0.5, Reynolds number Re=4.4186×10^6 based on MAC, and the range of AoA from -11° to 16°. The thickness of the first layer grid in the normal direction of the object surface is 3.78×10^{-5} to ensure that the $y^+<1$ in the first layer grid, and the growth rate of the boundary layer grid is 1.15.

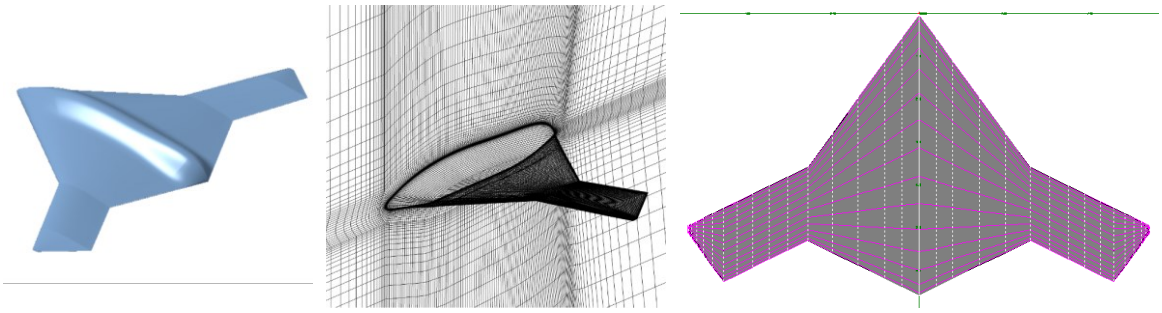

(a) geometry (b) mesh for RANS (c) mesh for VLM

Figure 6 – The geometry and mesh of flying wing UAV

The longitudinal aerodynamic characteristics of the flying wing is obtained using two numerical methods, as shown in Figure 7. Before the flying wing gets stalled, the aerodynamic of flying-wing is normal, which means that a large enough available linear region of aerodynamic characteristic is existed during the cruise status. The lift and drag and pitch moment of flying-wing calculated by the VLM are close to those calculated by the RANS, and its slope of lift line and longitudinal static stability obtained by the VLM are also consistent with the RANS results. When the angle of attack is up to 10°, the aerodynamic characteristics of flying wing is worsened with the flying wing stalled and the appearance of the inflexion of pitch moment curve. Compared the circulation distributions of flying wing calculated through the VLM and RANS at C_L=0.3, as shown in Figure 8, although there are some differences between two methods, but the variation trend and the magnitude of the local circulation of them along the span is basically consistent.

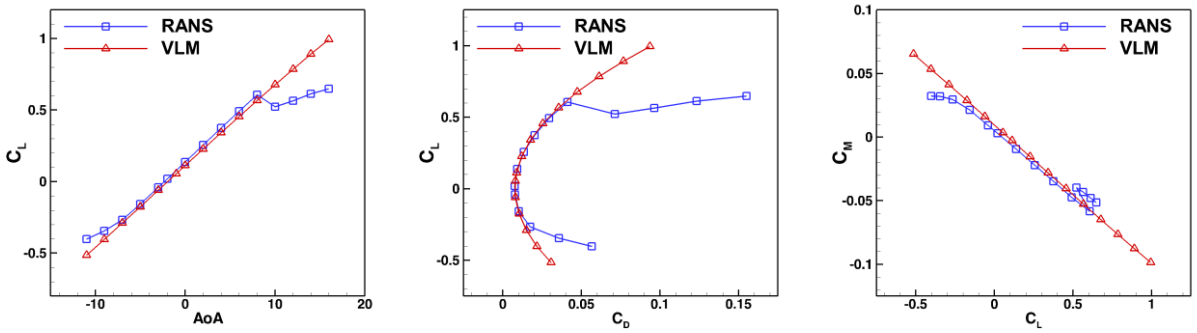

(a) AoA-C_L (b) C_L-C_D (c) C_L-C_m

Figure 7 – The longitudinal aerodynamics of single flying wing

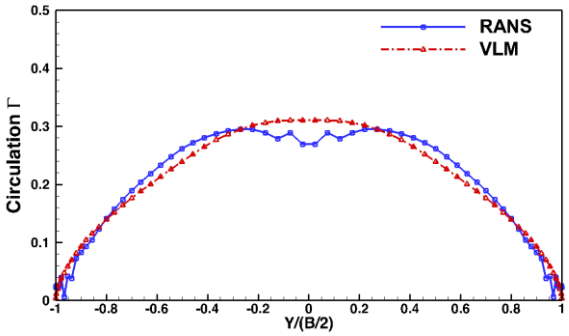

Figure 8 – The circulation distribution along the spread direction on the flying wing

The pressure and aerodynamic load distributions at the same lift condition at some profiles on the flying wing are obtained using VLM and RANS, as shown in Figure 9. The contour of the aerodynamic load on the flying wing using VLM is shown in Figure 10. The curvature line of the airfoils of the flying wing are designed to the S-shape in order that the lift on the tail of the wing is negative, which is used to decreased the pitch moment. Although the difference of the aerodynamic load between the results of VLM and those of RANS is increased for the flying wing, especially on the head of the flying wing, the variation trend of the aerodynamic load along the chord direction is still captured accurately by VLM.

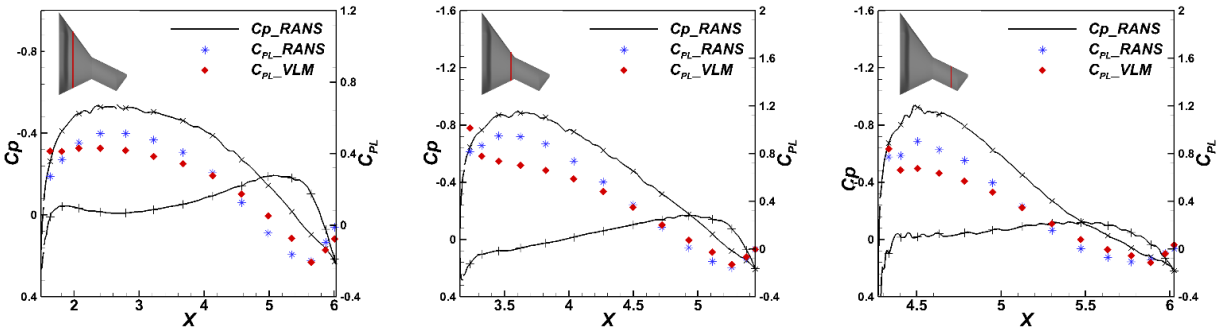

(a) Y/B=0.1 (b) Y/B=0.25 (c) Y/B=0.4

Figure 9 – The pressure distribution and aerodynamic load distribution at different profiles

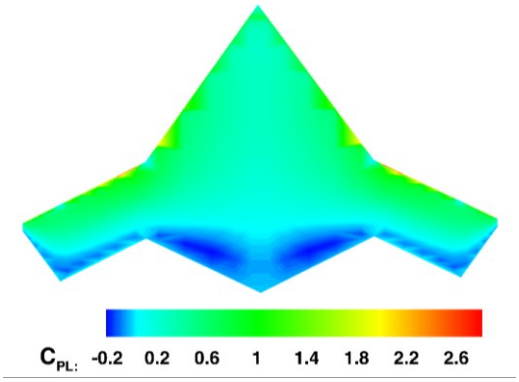

Figure 10 – The contour of aerodynamic load on the flying wing

3. Sensitivity analysis of the formation parameter

The significant aerodynamic coupling is existed between the captain and the follower in the close formation flight. In order to further explore the variation of the aerodynamic performance of aircraft in formation with the formation parameters, the sensitivity analysis of the aerodynamic performance of aircraft in formation with respect to the formation parameters is carried out, and the influence of the formation parameters on the aerodynamic performance of each aircraft in the formation is summarized.

The formation parameters (X_T, Y_T,Z_T) is established to describe the shape of formation through the

relative dimensionless distance in three directions of the follower to the captain, such as longitudinal (*x* axis direction), spread direction (*y* axis direction) and vertical direction (*z* axis direction), as shown in Figure 11. The relative coordinates system is established to describe the relative distance between them. The origin of coordinate is set on the nose of captain, the *x* axis is parallel to the chord of the flying wing with the positive direction from nose to the tail; the *y* axis is perpendicular to the symmetrical plane of the flying wing with the positive direction that points to the right in the insight of pilot; the *z* axis is defined by the right hand system with the positive direction pointing to up.

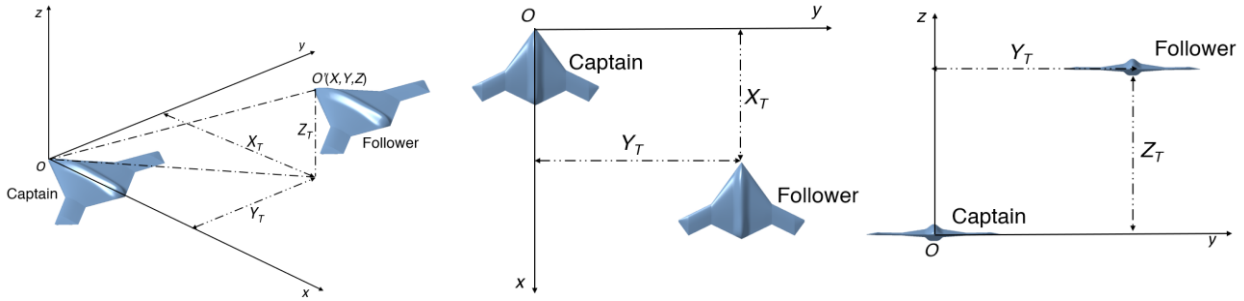

Figure 11 – The definitions of formation parameter and refer coordinate system

3.1 The variation along the longitudinal variation

The relationship between the aerodynamic of aircrafts in formation and the longitudinal formation parameter in the close formation flight is shown in Figure 12. The follower in the formation will convent to the captain when the longitudinal formation parameter X_T is negative. Therefore, the curve of the aerodynamic represents the aerodynamic of the captain when the longitudinal formation parameter X_T is negative while it represents the aerodynamic of the follower when the longitudinal formation parameter X_T is positive. The Aerodynamics of captain and follower in formation is changed greatly when the longitudinal formation parameter X_T changes from 0 to 1, and the variation amplitude of their aerodynamics will get more violent as they get closer. The aerodynamic influence of follower tends to be stable gradually when the longitudinal formation parameter X_T changes from 1 to 2, and the cruise AoA and drag of the captain is increased while the pitch moment is decreased, and the side force, roll and yaw moment caused by the follower gradually disappear in the process.

The variation of the aerodynamic of the follower with the longitudinal formation parameter X_T is more complicated. For the follower close to the captain along the spread direction ($Y_T < 0.6$) and another follower away from the captain along the spread direction ($Y_T > 0.6$), the aerodynamic of them will tend to be stable as the longitudinal formation parameter X_T increase, but the changing trend of aerodynamic of them is opposite. When the follower is close to captain, such as $Y_T = 0$, due to the downwash caused by the wake from captain, the AoA and drag of the follower increases while the pitch moment of the follower decreases as the longitudinal formation parameter X_T increase. The side force, roll and yaw moment of the follower are all 0 at $Y_T = 0$ because of symmetrical airflow. The situation is just the opposite when the follower is away from the captain.

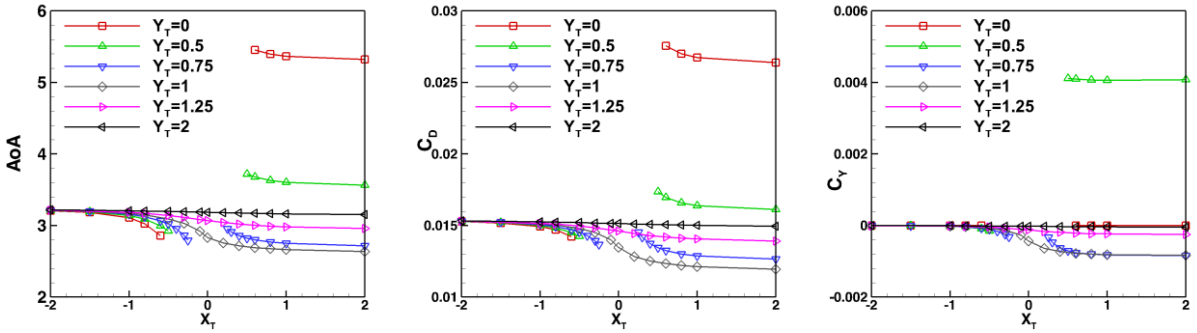

(a) X_T-AoA (b) X_T-C_D (c) X_T-C_Y

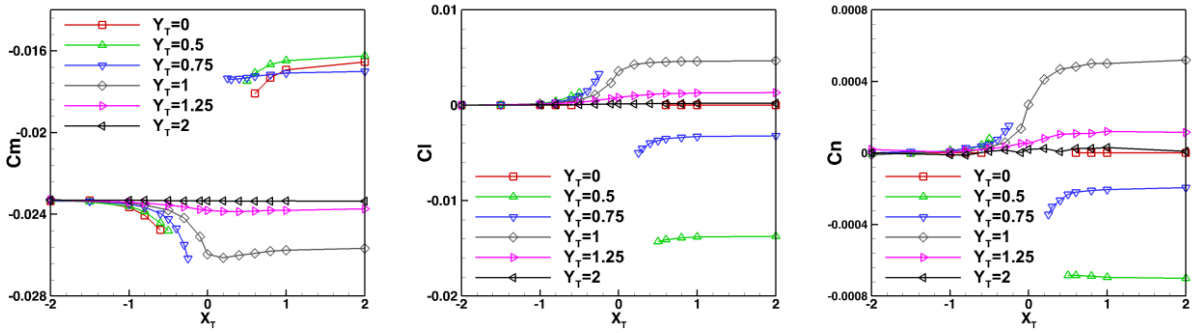

(d) X_T-C_m (e) X_T-C_l (f) X_T-C_n

Figure 12 – The variation of aerodynamic of follower with X_T at Z_T=0

Furthermore, the variation of longitudinal aerodynamic characteristics of the captain and follower in formation with the different longitudinal formation parameter X_T is analyzed at Y_T=0 and Z_T=0. The longitudinal aerodynamic characteristics of them is calculated using VLM at the condition where the cruise Mach number is 0.5 and the range of AoA is 0-14°, the results are shown in Figure 13.

As shown in Figure 13, the aerodynamics characteristics of the captain are slightly improved at X_T=0. The lift, the slope of lift line and the maximum of lift-drag ratio are increased slightly while the drag is decreased slightly, the longitudinal static stability is remained unchanged. However, the aerodynamics characteristics of the follower are worsened at X_T=0 due to the serious downwash from the wake of captain. The lift, the slope of the lift line, the maximum of lift-drag ratio and the longitudinal static stability are all decreased significantly while the drag and the pitch moment are increased. As the longitudinal formation parameter X_T increases from 0 to 2, the aerodynamic gain of the captain will be decreased to 0 gradually. The aerodynamics loss of the follower is also weakened, the lift and lift line slope are slightly increased while the drag is slightly reduced, and the longitudinal static stability is nearly unchanged in the process. But the aerodynamic loss of the follower will be exists in a long distance because the wake vortex needs to be dissipated for a long time along the longitudinal direction.

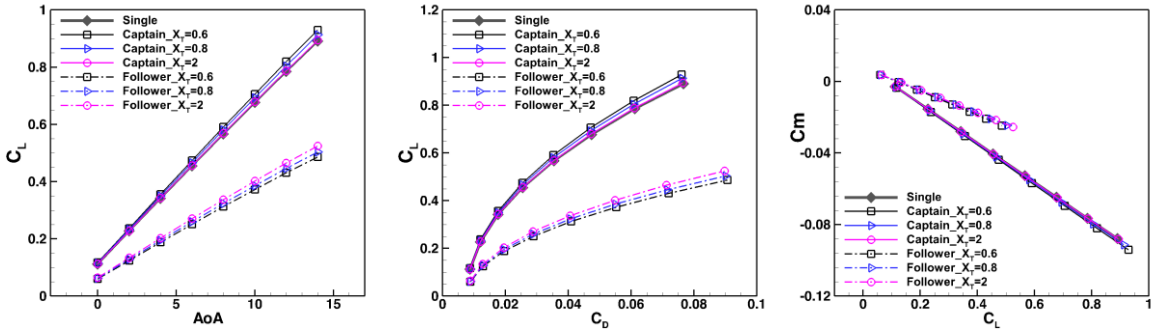

(a) AoA-C_L (b) C_D-C_L (c) C_L-C_m

Figure 13 – The longitudinal aerodynamic characteristics of the aircrafts at Y_T=0 and Z_T=0

The circulation distributions at AoA =3° and C_L =0.3 of both the captain and follower in formation at X_T =1,2, Y_T=0 and Z_T=0 are extracted in Figure 14 . As shown in Figure 14 (a), when the captain, follower and single flying wing are in same AoA, the local circulation of the follower along the spread direction is lower than that of both the captain and the single flying wing because the whole surface of the follower is in the downwash from the wake of the captain. While when these aircrafts are at the same C_L=0.3, the local circulation of the follower along the spread direction will be increased as the AoA of the follower is increased to meet the same requirement of the C_L=0.3, as shown in in Figure 14 (b). The local circulations of the follower in the outer wing section and the central body region are larger than that of the captain while the local circulations of the follower in the inner wing section is smaller than that of the captain in order to keep the total lift of them same on both aircrafts.

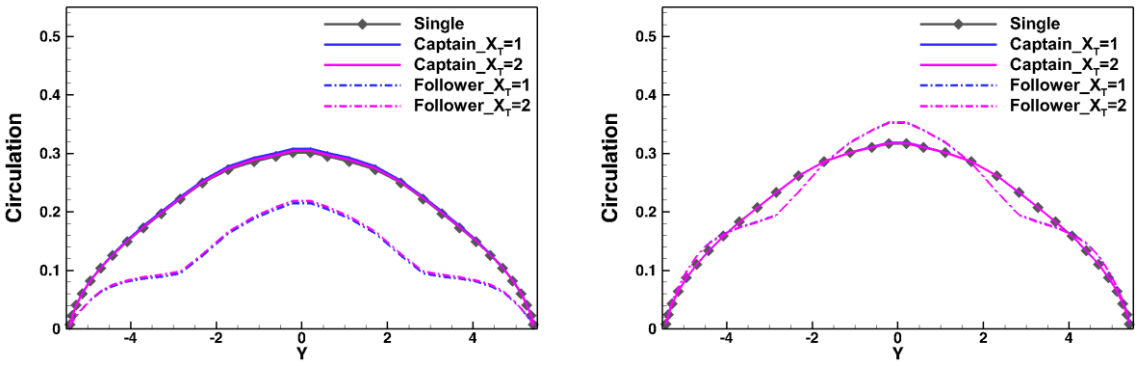

(a) AoA=3° (b) C_L=0.3

Figure 14 – The circulation distributions of aircrafts in formation at Y_T=0 and Z_T=0

3.2 The variation along the vertical direction

The variation of aerodynamics of captain in formation with vertical formation parameter Z_T in close formation flight is analyzed in detail as shown in Figure 15, such as the cruising AoA, drag, pitch moment and roll moment on the captain. The side force and yaw moment on the captain are not shown here because they are almost unaffected by the follower. The aerodynamic of the captain will be improved slightly due to the effect of the follower, and the maximum aerodynamic gain of the captain can be obtained at YT=0 and ZT=0 where the AoA of the captain is decreased by 0.1 and the drag is reduced by 4 counts. It shows that the effect of the follower on the aerodynamic of captain is existed but its amplitude is limited.

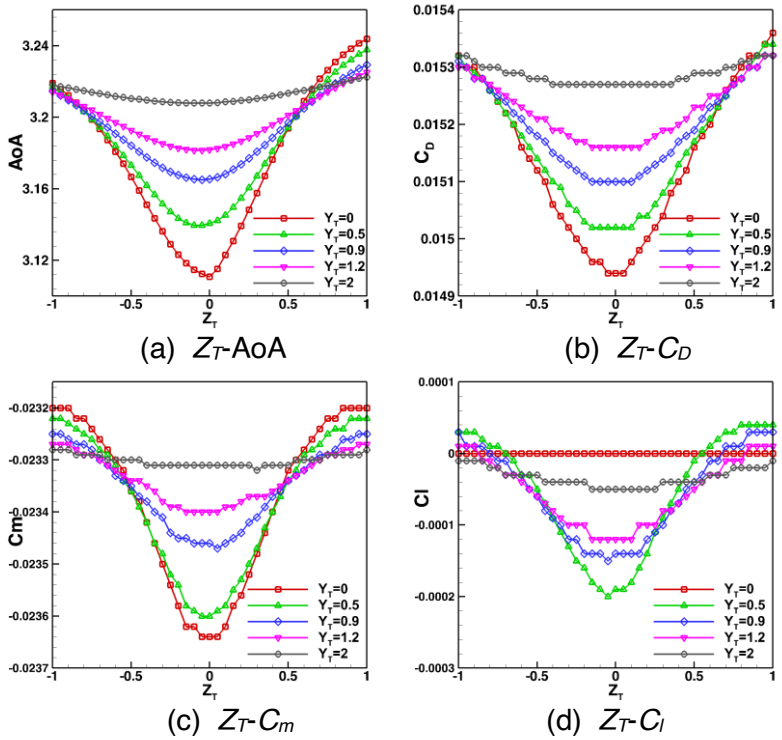

(a) Z_T-AoA (b) Z_T-C_D

(c) Z_T-C_m (d) Z_T-C_l

Figure 15 – The variation of aerodynamic of the captain with Z_T at X_T =1

Next, the variation of aerodynamics of the follower with vertical formation parameter Z_T in close formation flight is analyzed in detail as shown in Figure 16, the most serious effect of the captain on the aerodynamics of the follower is occurred at the Z_T=0 where the follower is located in the plane of wake vortex core of the captain. As the vertical formation parameter Z_T increases or decreases from 0, the follower is less affected by the captain because the follower moves away from the wake vortex of the captain gradually. The change of the vertical formation parameter Z_T cannot make the upwash

convert to the downwash or make the downwash convert to the upwash, just only can enable the follower approach to or move away from the plane of wake vortex core with the effect of the captain on the follower enhanced or weakened. Therefore, when the Z_T is closing to 0, the aerodynamics gain of the follower under the upwash will be increased, such as at Y_T=0.9, while the aerodynamics loss of the follower under the downwash will be decreased, such as at Y_T=0.

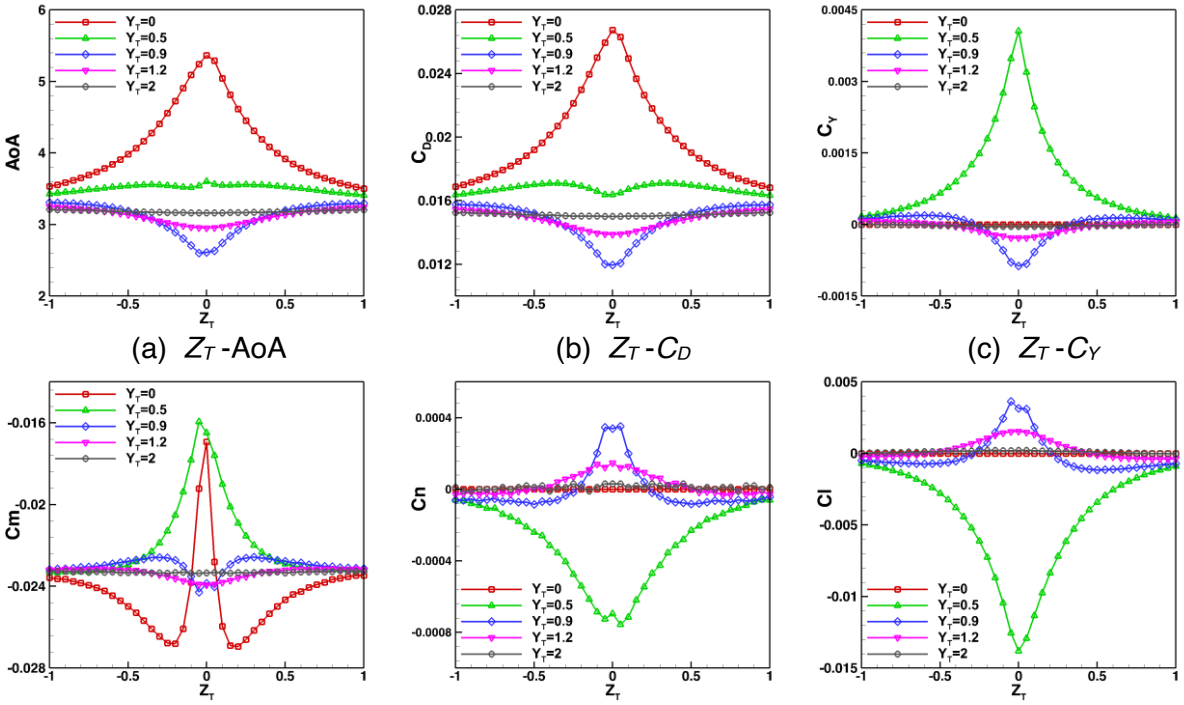

(a) Z_T-AoA (b) Z_T-C_D (c) Z_T-C_Y

(d) Z_T-C_m (e) Z_T-C_l (f) Z_T-C_n

Figure 16 – The variation of aerodynamic of the follower with Z_T at X_T =1

Furthermore, the variation of longitudinal aerodynamic characteristics of the follower with the vertical formation parameter Z_T is analyzed at X_T=1 and Y_T=0.9, as shown in Figure 17.

As Z_T is increased or decreased from 0, correspondingly the follower moves away from the plane of the wake vortex core, the lift, the slope of the lift line and the maximum lift-drag ratio for the follower are decreased while the drag is increased. With the increase of the vertical formation parameter Z_T, the effect of wake vortex of the captain on the follower is gradually disappeared, and the longitudinal aerodynamic characteristic of the follower is gradually closing to that of the single flying wing. Luckily, the longitudinal static stability of the follower is unchanged in the process, which is very beneficial to flight control.

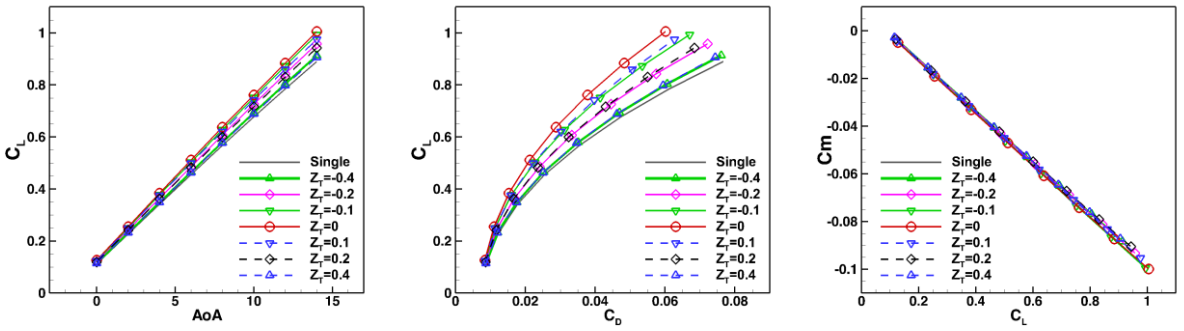

(a) AoA-C_L (b) C_D-C_L (c) C_L-C_m

Figure 17 – The longitudinal aerodynamic characteristics of the follower at X_T =1 and Y_T=0.9

3.3 The variation along the spread direction

The variation of aerodynamic of aircrafts in formation with spread formation parameter Y_T in close

formation flight is analyzed in detail as shown in Figure 18. The aerodynamics of the captain are slightly improved as the follower move close to the captain along the spread direction. The cruise AoA and cruise drag of the captain is slightly reduced and the pitch moment is slightly decreased when the longitudinal and spread formation parameter X_T and Y_T are both small, meanwhile the side force, row and yaw moment of the captain is nearly not changed. However, the aerodynamic of the follower in formation is changed significantly and the trend of its variation is more complicated which needs to be analyzed in detail. For the follower of the formation at the cruise C_L=0.3, its cruise drag is mainly depended on its cruise AoA, the cruise drag of the follower will be increased with the increase of its cruise AoA, and vice versa. As the follower moves outward from Y_T=0 to Y_T=1 along the spread direction, the wake flow of the captain acting on the follower is converted from the initial downwash flow to the upwash flow. And with the further outward movement of follower from Y_T=1 to Y_T=2, the effect of the wake of the captain on the follower is reduced to 0 gradually. Therefore, in the process from Y_T=0 to Y_T=2, the induced AoA on the follower will be changed from negative to positive, and then reduced to 0. In order to keep the same lift for cruise, the cruise AoA of the follower will be decreased from 5.4 to 2.6, and then return slowly to 3.2, correspondingly the cruise drag is reduced from 270 counts to 120 counts and then restores to 150 counts that is same as the drag of the single flying wing.

One conclusion drawn from the Figure 18 is that the position with the minimum drag for the follower occurs with the wingtip slightly overlapping the center of the incoming vortex (Y_T=0.9). This is easily understood. The local contribution to the induced drag is proportional to the product of the vertical induced velocity component and the local circulation. Since local circulation approaches zero at the wingtip, it is advantageous (in terms of drag reduction) to shift the large regions of upwash to sections on the wing with higher circulation. However, this shift in positioning should not be taken too far because downwash is produced inboard of the vortex center, which would increase the induced drag of the follower in formation.

The variation of the side force and pitch moment of the follower with the spread formation parameter Y_T is more complicated due to the wash flow from the wake of the captain, as shown in Figure 18(c)(d). The side force of the follower is increased as the Y_T increases from 0 to 0.4, and is reduced from positive to negative minimum as the Y_T increased from 0.4 to 0.9, and is gradually restored to 0 as the Y_T increased from 0.9 up to 2. In the process of the increase of the Y_T from 0 to 2, the pitch moment of the follower is oscillating with a large amplitude around 0. It is decreased to a negative minimum at Y_T=0.3, increased to a positive at Y_T=0.6 and decreased again to a negative second minimum at =0.9, then slowly restored to 0 as Y_T increased to 2. The pitch moment of the follower is very sensitive to the spread formation parameter and is changed non-monotonously in close formation flight. The large oscillation of the pitch moment of the follower will be appeared with the amplitude of 50% due to a little change in the spread formation parameter, which is extremely disadvantageous to flight control.

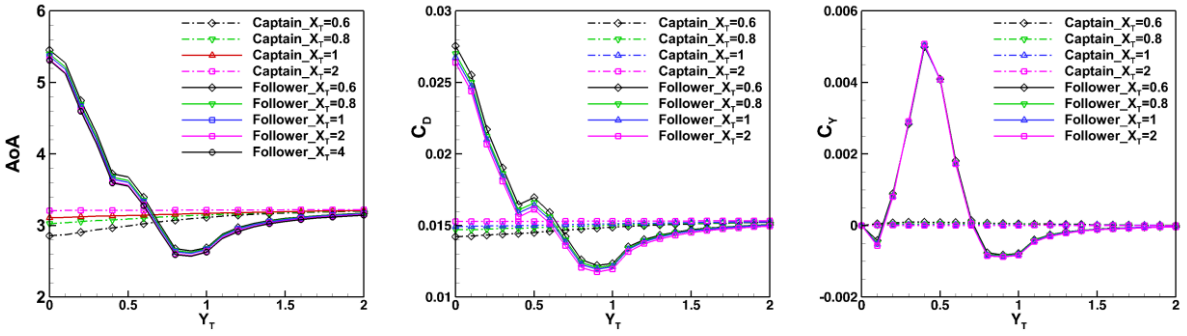

(a) Y_T-AoA (b) Y_T-C_D (c) Y_T-C_Y

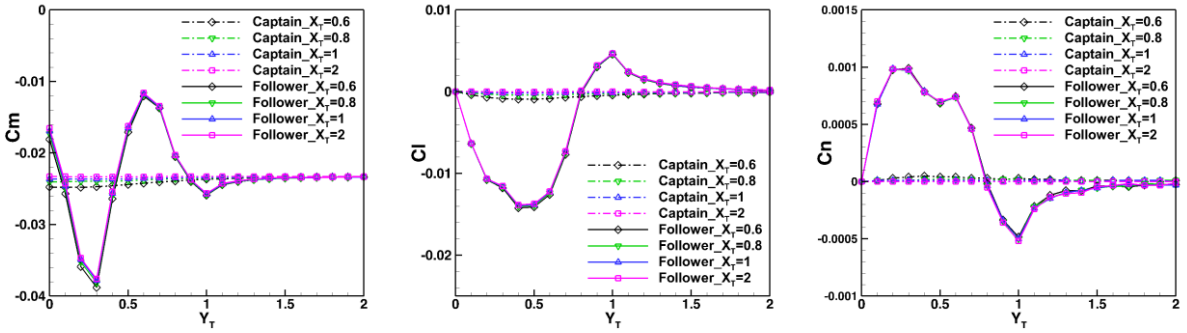

(d) Y_T-C_m (e) Y_T-C_l (f) Y_T-C_n

Figure 18 – The variation of aerodynamic of aircrafts in formation with Y_T at Z_T=0

The circulation distributions of the captain and follower in formation at X_T=1, Y_T=0.5, 1 and Z_T=0 are shown in Figure 19 in order to explain the variation of the roll and yaw moment of the follower with the spread formation parameter Y_T that are shown in Figure 18(e)(f). The lift on the left wing of the follower is less than the lift on its right wing and it will roll to the left because of the downwash from captain when the follower is close to the captain along the spread direction ($Y_T \leq 0.8$). The phenomenon is just the opposite because of the upwash from the captain when the follower is far away from the captain along the spread direction ($Y_T \geq 0.8$). As for yaw moment of the follower, its variation is mainly affected by the drag on the wing. The drag on the left wing of the follower is less than the drag on its right wing and it will yaw to right when $Y_T \leq 0.8$ and it will yaw to the left when $Y_T \geq 0.8$ because of the effect from captain.

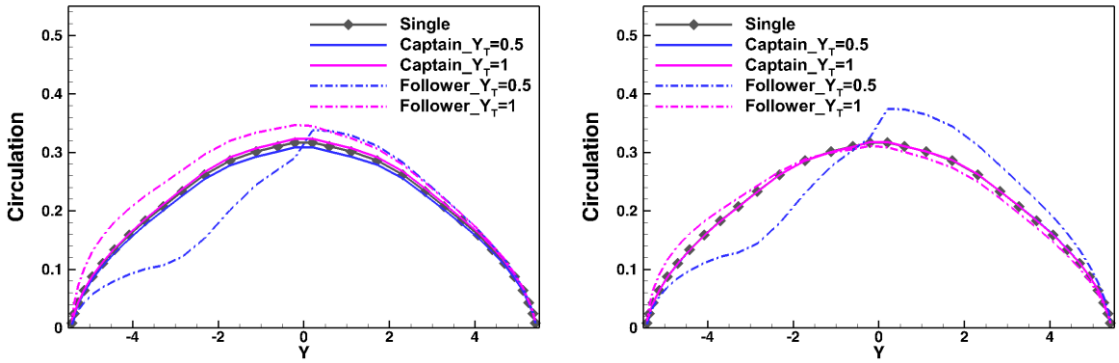

(a) AoA=3° (b) C_L=0.3

Figure 19 – The circulation distribution of the aircrafts in formation at X_T=1 and Z_T=0

The longitudinal aerodynamic characteristics of the follower in formation at X_T =1 and Z_T=0 is further analyzed, as shown in Figure 20. The cruising Mach number of the formation is 0.5, and the range of AoA on the follower is 0°-14°. The aerodynamic characteristics of the follower will be deteriorated significantly when the follower is under the downwash from the wake of the captain, such as at Y_T = 0 and Y_T = 0.5. Compared to the aerodynamics of the single flying wing, the lift and the slope of lift line of the follower are decreased at the same AoA, the drag and the pitch moment of the follower are increased while the maximum lift-drag ratio is decreased at the same lift. Further, even the longitudinal static stability of follower is decreased, as shown in Figure 20(d). On the contrary, the aerodynamic characteristics of the follower will be improved slightly when it is under the upwash from the wake of the captain, such as at Y_T = 0.9 and Y_T = 1.2. Compared to the aerodynamics of single flying wing, the lift and the slope of lift line of the follower are increased at the same AoA, the drag and the pitch moment of the follower are decreased while the maximum lift-drag ratio is increased at the same lift, the longitudinal static stability is unchanged. The effect of the captain on the follower will be disappeared and the aerodynamic characteristics of the follower will be close to that of the single flying wing when the Y_T = 2 and even Y_T > 2.

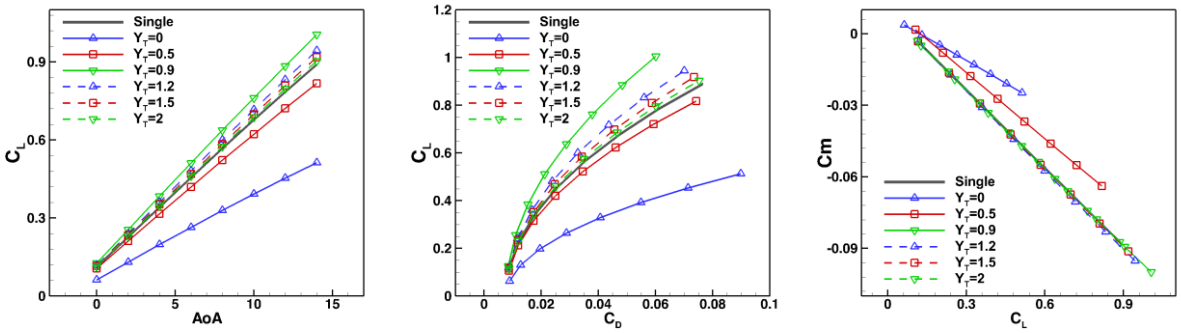

(a) AoA-C_L (b) C_D-C_L (c) C_L-C_m

Figure 20 – The longitudinal aerodynamics of the follower in formation at X_T =1 and Z_T=0

In order to explain the variation trend of the aerodynamics with the formation parameters more clear. Compared to the aerodynamic load on the single flying wing, the aerodynamic load deviation on the aircraft in formation is defined as:

$$\left(\Delta C_{PL}\right)_j = \left(C_{PL}\right)_j^{formation} - \left(C_{PL}\right)_j^{single} \tag{17}$$

where the superscript *formation* represents the aircraft in formation, such as captain and follower, the superscript *single* represents the single aircraft. The subscript *j* represents the *j*-th grid element on one aircraft.

The contour of the aerodynamic load deviation on the captain and follower in formation at different spread formation parameters are given in Figure 21. In order to evaluate the effect of the wake vortex on the aerodynamic load on the wing of the follower, the AoA of the captain and the follower in formation are both set to 3° that is same as the AoA of the single flying wing. As the spread formation parameters Y_T is increased while the longitudinal and vertical formation parameter X_T, Z_T are kept as constant, the aerodynamic load deviation on the captain in formation is nearly equal to 0, which meaning that the aerodynamic load on the captain is almost unaffected by the follower and is nearly same as that on the single flying wing. However, the follower in formation is deeply affected by the wake vortex of the captain, the negative aerodynamic load deviation is dominated on the follower because of the downwash when the spread formation parameter Y_T<0.5, which lead to the lift loss and the drag increase. The positive aerodynamic load deviation is dominated on the follower and the aerodynamic performance of the follower is improved when the spread formation parameter Y_T>0.5.

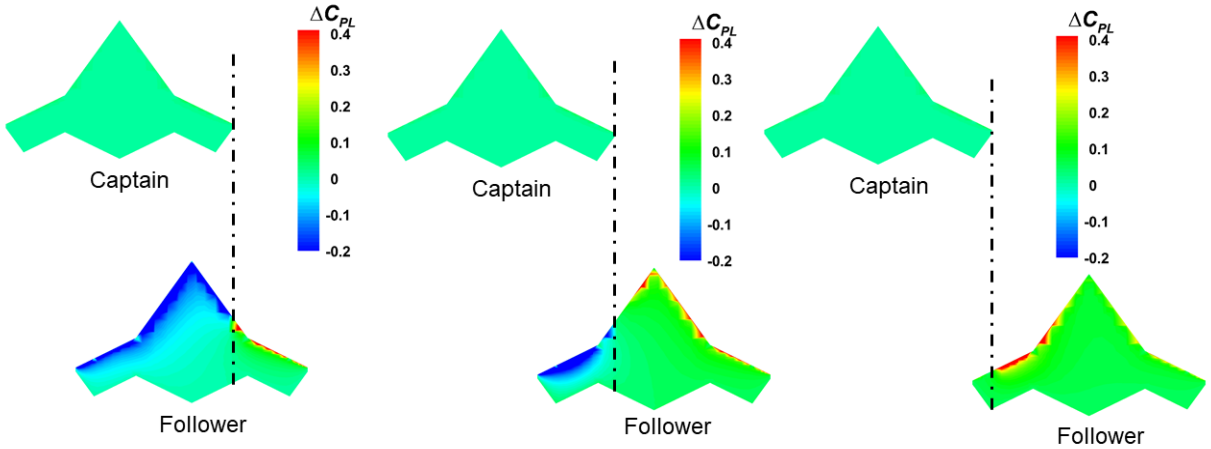

(a) Y_T=0.3 (b) Y_T =0.6 (c) Y_T =0.9

Figure 21 – The contour of aerodynamic load deviation for aircrafts in formation

Of particular concern is that the region of the follower where the aerodynamic load is affected significantly by wake vortex is mainly focused on the head area of the lifting surface that is in front of the center of gravity. It is the reason why the pitch moment of the follower will be changed violently

with the formation parameters. On this region, the violent increase of the lift caused by upwash is acted in front of the center of gravity and leads to the violent increase of the pitch moment, and vice versa.

4. Conclusion

The overall performance of aerodynamic and combat will be improved significantly through the reasonable formation flight. In this paper, A formation composed of two flying-wing UAVs is selected to explore the effect of formation parameters on the aerodynamic characteristics of aircrafts in formation using VLM. The aerodynamic characteristics of the single flying-wing UAV are analyzed and evaluated using VLM whose accuracy are verified by the high-precision RANS. The sensitivity analysis of the formation parameters for aircrafts in close formation flight is carried out using VLM. The variation rules of the aerodynamics on aircrafts with the formation parameters are summarized, which can be used to guide the formation design.

The longitudinal formation parameter X_T reflects the evolution of the wake vortex along the flow direction. The effect of the wake vortex on the follower will be stable when the X_T is great than 1.

The vertical formation parameter Z_T determines the relative distance between the follower and the plane of wake vortex core, the largest aerodynamic gain can be obtained at Z_T=0.

The spread formation parameter Y_T determines whether the follower can be in the upwash of the wake vortex from the captain and obtain the aerodynamic gain. The drag of the follower can be reduced significantly with the slight fluctuation when the Y_T is in the range from 0.8 to 1.0.

The aerodynamic load deviation produced by the formation flight is focused on the head of the lifting surface which is in front of the center of gravity, which leads to the violent variation of the pitch moment on the wing with the formation parameters.

5. Contact Author Email Address

mailto: junqiang@nwpu.edu.cn

6. Copyright Statement

7. References

[1] Bajec I L, and Heppner F H. Organized flight in birds. *Animal Behaviour*, Vol. 78, No. 4, pp 777–789, 2009.

[2] Lissaman P B, and Shollenberger C A. Formation flight of birds. *Science*, Vol. 168, No. 3934, pp 1003–1005, 1970.

[3] Hummel D. "Aerodynamic aspects of formation flight in birds." *Journal of Theoretical Biology*, Vol. 104, No. 3, pp. 321–347, 1983.

[4] Hummel D. The use of aircraft wakes to achieve power reductions in formation flight. *AGARD FDP Symposium on The Characterization & Modification of Wakes from Lifting Vehicles in Fluid*, 1996.

[5] Wagner E, Jacques D, Blake W, and Pachter M. Flight test results of close formation flight for fuel savings. *AIAA Atmospheric Flight Mechanics Conference and Exhibit*, Monterey, California, 2002.

[6] Vachon M J, Ray R, Walsh K, and Ennix K. F/A-18 Aircraft performance benefits measured during the autonomous formation flight project. *AIAA Atmospheric Flight Mechanics Conference and Exhibit*, 2002.

[7] Pahle J, Berger D, Venti M, Duggan C, Faber J, and Cardinal K. An initial flight investigation of formation flight for drag reduction on the C-17 aircraft. *AIAA atmospheric flight mechanics conference*, 2012.

[8] Bieniawski S R, Rosenzweig S, and Blake W B. Summary of flight testing and results for the formation flight for aerodynamic benefit program. *52nd Aerospace Sciences Meeting*, 2014.

[9] Maskew B. Formation flying benefits based on vortex lattice calculations. 1977.

[10] Blake William B. An aerodynamic model for simulation of close formation flight. *AIAA Modeling and Simulation Technologies Confeerence and Exhibit*, Denver, Colorado, 2000.

[11] Ning S A, Flanzer T C, and Kroo I M. Aerodynamic performance of extended formation flight." *Journal of aircraft*,

Vol. 48, No. 3, pp. 855–865, 2011.
[12] Veldhuis L, Voskuijl M, and Fransen B. Formation flight-fine-tuning of theoretical performance prediction. *51st AIAA Aerospace Sciences Meeting including the New Horizons Forum and Aerospace Exposition*, 2013.
[13] Slotnick Jeffrey P. Computational aerodynamic analysis for the formation flight for aerodynamic benefit program. *52nd Aerospace Sciences Meeting*, National Harbor, Maryland, 2014.
[14] Zhang Qingrui and Liu Hugh H T. Aerodynamics modeling and analysis of close formation flight. *Journal of Aircraft*, Vol. 54, No. 6, pp. 2192–2204, 2017.
[15] Caprace Denis-Gabriel, Winckelmans Gregoire S, Chatelain Philippe, and Eldredge Jeff. Wake vortex detection and tracking for aircraft formation flight. *AIAA Aviation 2019 Forum*, Dallas, Texas, 2019.